Optik - International Journal for Light and Electron Optics 306 (2024) 171800

Contents lists available at ScienceDirect

Optik

journal homepage: www.elsevier.com/locate/ijleo

Curcumin analogue: Synthesis, DFT and nonlinear optical studies

Ayman G. Faisal [a], Qusay M.A. Hassan [b,*], Tahseen A. Alsalim [c,*], H.A. Sultan [b], Fadhil S. Kamounah [d], C.A. Emshary [b], Kawkab Ali Hussein [c]

[a] Department of Applied Marine Sciences, College of Marine Sciences, University of Basrah, Basrah 61001, Iraq
[b] Department of Physics, College of Education for Pure Sciences, University of Basrah, Basrah 61001, Iraq
[c] Department of Chemistry, College of Education for Pure Sciences, University of Basrah, Basrah 61001, Iraq
[d] Department of Chemistry, University of Copenhagen, Copenhagen, Denmark

ARTICLE INFO

Keywords:
Curcumin analogue
Mullikan charges
DFT
DPs
Z-scan
All-0ptical switching

ABSTRACT

The synthesis of a new curcumin analogue dye via 3-chloro-2,4-pentanedion condensing with an aromatic aldehyde is considered. Following that, the synthesized compound is diagnosed utilizing spectroscopic methods, including FTIR, mass, ^{1}H NMR, and ^{13}CNMR. The curcumin analogue geometric optimization and theoretical studies are conducted on thermodynamic properties using DFT. The B3LYP techniques, which are hybrid functional with a 6–311+G(d) as the basis set, are adopted to compute the HOMO, LUMO, and Mullikan atom charges of the studied compound. The curcumin analogue dye nonlinear optical (NLO) properties are examined under excitation with a 473 nm, low power, cw and TEM_{00} mode laser beam. The index of nonlinear refraction (INLR) and coefficient of nonlinear absorption (CNLA) are estimated using diffraction patterns for the former and Z-scan for the latter. The INLR reaches a value as high as 6.86×10^{-11} m^2/W, while the CNLA reaches 2.23×10^{-3} cm/W. All-optical switching (AOS) is tested in the novel curcumin analogue dye using two methods: static AOS and dynamic AOS.

1. Introduction

Laser beam self-interaction in a medium occurs due to the changes in the medium optical properties created via incident radiation. During the last three decades, considerable interest has been paid to problems concerning the nonlinear interaction of a Gaussian laser beam with a nonlinear medium (NLM) such as self-defocusing (SDF), self–phase modulation (SPM) and self-focusing (SF) can be observed. For example, a ring intensity distribution patterns can be induced. The technique known as the diffraction patterns (DPs) can be used in determining, the index of nonlinear refraction, INLR [1]. Self–phase modulation (SPM) effect is attributed to the refractive index dependent on intensity. Such effect was observed in a number of systems [2–5]. When a laser beam transvers an NLM, the beam spot size varies in area based on SF or SDF, so when drawing the beam power transmitted through a narrow iris against the sample position relative to the lens focus (±z), a peak then a valley resulted when the medium showed SDF, and a valley then a peak resulted when the system showed SF. Such a technique is known as Z-scan, discovered by Sheik-Bahae et al., in 1989–1990 [6,7], where it can be used to estimate the coefficient of nonlinear absorption (CNLA) as well as the INLR.

Organic dyes and organic compounds offer unique applications in the areas of optical computing, harmonic creation, optical power limiting, optical switching, optical communications, and optical storage, because they show nonlinear optical (NLO) features [8–12].

* Corresponding authors.
E-mail addresses: qusayali64@yahoo.co.in (Q.M.A. Hassan), tahseen.alsalim@uobasra.edu.iq (T.A. Alsalim).

https://doi.org/10.1016/j.ijleo.2024.171800
Received 1 March 2024; Received in revised form 4 April 2024; Accepted 4 April 2024
Available online 17 April 2024

In addition to the various experimental approaches, theoretical simulations have recently been used begin a method for calculating the NLO characteristics of organic compounds [13,14]. The advantages of computational approaches include prior knowledge of how structure affects characteristics and the parameters influencing the effectiveness of NLO properties, for instance, the role of acceptor /donor fragments inside the molecule and the effect of solvent [15,16].

Curcumin longa is a perennial herb. It is an important medicinal and aromatic plant considered as one of the gold resources with massive export prospects as medicine, cosmetics, and cooking spice dye [17]. Curcumin is derived from the rhizomes of Curcuma longa. It is the major active component of turmeric long, used as a coloring agent and as a spice in curry in pharmaceuticals, yellow mustards, hair dyes, and cosmetics. It has received a lot of attention for its potential cancer chemo-preventive, antioxidant, and anti-inflammatory properties [18–20]. Curcumin is used in the synthesis of dihydropyridones [21,22],2,3-dihydro-4-pyridiniones [23], etc. It is used in dye solar cells [24], ZnO nanoparticle-based dye solar cells [25], as a therapeutic agent [26], and other applications. Different types of curcumin and their derivatives, such as dimethoxy curcumin and chloro-curcumin, were investigated for their possible nonlinear properties [27,28]. Curcumin and its derivatives have been extensively studied such as a novel stabilizing and reducing agent [29], the derivation of some polyester from curcumin [30], as new mitochondrial coupling agents [31], inhibition of cellular reaction oxygen species generation [32], study of its photo-physical, photo chemistry and photobiological properties [33,34], and its NLO properties [35].

The synthesis of second-order organic NLO materials has successfully utilized donor-acceptor molecules [36–38]. They typically exhibit strong linear and NLO characteristics and are donor-acceptor (push-pull) chromophores. By adjusting the relative orientation of the acceptor and donor cores, their initial hyperpolarizability, βo, values may be raised [39].

In this article, we describe the synthesis procedure of curcumin analogue dye and its nonlinear optical (NLO) properties, viz., the index of nonlinear refraction (INLR) and the coefficient of nonlinear absorption (CNLA) under interaction with 473 nm, low power cw and TEM_{00} laser beam based on the diffraction patterns (DPs) and the Z-scan. All optical switching (AOS) is examined in the compound using two laser beams viz., 473 nm and 532 nm.

2. Experimental

2.1. Instrumentation

Fluka, Merck, Sigma, and Fischer provided the first ingredients, solvents, and reagents. Shimadzu FTIR (affinity-1) used to record IR spectra in the 400–4000 cm^{-1} range, and Brucker 400 spectrometer was used to analyze ^{1}H and ^{13}CNMR spectra while using tetramethylsilane (TMS) as an internal standard together with dimethyl sulfoxide-d6 as the solvent. The chemical shifts, δ, in ppm coupling and constants measured in Hz. Mass spectra were scanned at 70 eV with an Agilent 5975 C spectrometer using the EI technique.

2.2. Synthesis procedure of symmetric curcumin analogue

In the reaction vessel, 1.093 g (0.0155 mol) of boric oxide and 2 g (0.0155 mol) of chloroacetylaceton were mixed for an hour with 30 ml of DMA. 1,4-Benzodioxan-6-carboxaldehyde (0.031 mol) was added with dry DMA to the mixture, heated in a water bath to 80°C, and then trimethylborate (3.23 g) (0.031 mol) was added to the reaction. After stirring the mixture for a few minutes, the solution of n-butylamine 0.5 g (0.006 mol) in 30 ml of DMA was gradually added over an hour. Four more hours were spent stirring the mixture. Overnight the reaction mixture was left. The mixture was agitated for an hour after the addition of 5% acetic acid (43 ml) at 80°C. As the mixture cooled, the solid component was separated using filtration, twice-washed in hot distilled water, dried, and then recrystallized using ethanol.

2.2.1. (1E,6E)-4-chlor0-1,7-bis(2,3-dihydrobenzo[b][1,4]dioxin-6-yl)hepta-1,6-diene-3,5-dione (cur-oxohexa)

Recrystallized orange crystal, from ethanol,yield 65%, M.P. 202–205 °C.^{1}HNMR (DMSO, δ ppm): 4.31(8 H, dd, *J*=4, -OCH_2-CH_2O-protons), 6.94(2 H, d, *J* =8, olefinic proton), 7.52 (2 H, Ar-H), 7.68 (2 H, d, *J*=4, Ar-H), 7.86 (2 H, d, *J*=4, Ar-H), 8.25(2 H, d, *J*= 8, olefinic proton).^{13}C

NMR (DMSO, ppm), 185.5 (C═O), 144.8, 144.3, 144.4, 129.7, 129.5, 128.6, 127.3, 123.6, 120.5, 73.13(C-Cl),64.4(CH_2-CH_2) IR (υ, cm^{-}1): 3456 (enolic OH),3047 (Ar-H), 2972 (aliph H), 2877(aliph H), 1695 (C═O), 1583 (C═C), 1508(CH_2), 1288 (C-O),1255(CH-C═O bending), 1068 (C-O). MS: EI (70 eV, m/z), 426[M], 374, 297, 254, 189,149, 89, 64, 43.

2.3. Theoretical calculations of the curcumin analogue (cur-oxohexa)

The computation of thermodynamic parameters, molecule orbital characteristics, dipole moment, and molecular electrostatic potential properties are given more consideration in computer-aided quantum mechanical approaches. In order to optimize the structure of chemicals employed in the current study in the gas phase and forecast their various characteristics, the DFT method has been used. Employing the Gaussian 09 suite, we used the B3LYP (Becke's three-parameter hybrid functional) utilizing the L.-Y.-P. correlation function with a 6–311+G (d) basis set. Such level of theory is frequently employed in computer computations and offers precise geometric structures and frequencies of normal modes. The dipole moment, μ, E_{HOMO}, and E_{LUMO} energies, as well as chemical hardness, η, global electrophilic index, ω, softness, S, optical softness, So, electronegativity, χ, chemical potential, CP, and global nucleophilic index, N, were all calculated using the aforementioned formulae [40–42]:

$EA = - E_{LUMO}$ (eV)

$IE = - E_{HOMO}$ (eV)

$\eta = (IE - EA)/2)$ (eV)

$S = 1/\eta$ (eV) $^{-1}$

$S_o = S/2$ (eV) $^{-1}$

$\chi = (IE + EA)/2$ (eV)

$CP = -\chi$ (eV)

$\mu = E_{HOMO} + E_{LUMO}/2$

$\omega = \mu^2/2\ \eta$

$\Delta N_{max} = -\mu/\eta$

2.4. Experimental set up

Three experiments were conducted to study the NLO properties of curcumin analogue viz., the laser beam power input effect on the type of diffraction patterns (DPs), the wave front type effect of the laser beam on DPs, and temporal variation of DPs. To carry out these experiments, the following were used: a laser beam of 1.5 mm spot size as it leaves the device output mirror, with a power output range of zero to 66 mW and a wavelength 473 nm, a positive lens of 5 cm, 1 mm thickness glass cell, a semitransparent screen 30×30 cm, and a digital camera were used. In the first experiment Fig. 1, the 473 nm laser beam focused by the 5 cm focal length lens to 19.235 μm spot size. The sample cell was fixed at the lens focus. The transmitted laser beam travels a distance of 85 cm, then falls on the screen. Due to the laser beam passing through the sample that has a high absorption coefficient so that the medium absorbed appreciable amount of energy from the beam. When the power input is low a solid small bright spot appears first. By increasing the power input, spot area increased due to SDF. By gradually increasing laser beam power, rings appeared whose area and number increased until the ring pattern lost symmetry in the upper half as a result of vertically convection thermal current so that the upper part rings grew in a small ratio compare to the lower half i.e., the patterns compressed. In the second experiment, the sample cell fixed in two positions, i.e., 1 cm before / 1 cm after the lens focus. From basic geometrical optics, the beam front changes from convex (1 cm before) to concave one (1 cm after). It was noticed that patterns type differ due to the laser beam interaction with NLM result an effect noticed by Santamato and Shen as early as 1984 [43–45]. At an input power of 56 mW falling on the sample, the temporal evolution of the obtained DPs formed on the screen, where it was noticed that the pattern appeared as a solid bright spot of small size at t = 0 sec, then the area of the spot increased with time, then broke into rings whose number and area increased as time lapsed then started losing its symmetry in x-y plane so that the pattern became compressed in the upper half as a result of vertical convection thermal current.

The property of all-optical switching, AOS, was tested using 473 nm as the excitation beam or the controlling one and 532 nm of the same spot size of 1.5 mm and the later power varied in the range of 0–50 mW as the controlled beam. Laser beams were focused using two, 20 cm focal length lenses, and a 60×60 cm semitransparent screen was used where the laser beam fell. The medium absorption coefficient against the beam 532 nm, is small enough so that no DPs resulted since small amount of beam energy was absorbed by the NLM while the medium absorption coefficient against the beam 473 nm is high that the beam passage through the medium lead to the generation of DPs.When the two beams pass simultaneously through the medium, two DPs resulted, one for each beam (473 nm) and one due (532 mm) beam based on the phenomenon cross self- phase modulation (XSPM) that measure a change of light field phase due to other co-propagating fields [46–48]. The two beams traversed the nonlinear medium by the crossing passing technique [49–51] as shown in Fig. 2.

The INLR and the CNLA can be measured using the standard Z-scan technique [6,7]. The laser beam used was 473 nm. The same sample cell was fixed on a moveable stage and the screen replaced with a power meter covered with a 2 mm iris. The transmitted beam power through the NLM was measured by a power meter covered with the narrow,2 mm, iris, versus the sample position (±z) where the lens focus is at z = 0. This is the closed aperture, CA Z-scan. By replacing he iris with a positive lens the open aperture, OA, Z-scan, resulted. Fig. 3 shows the two Z-scan types viz., CA and OA Z-scan.

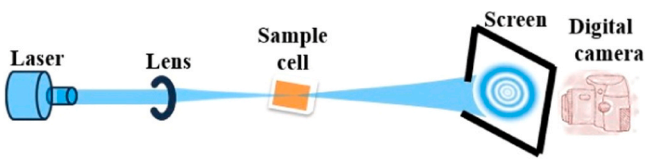

Fig. 1. DPs experimental set-up.

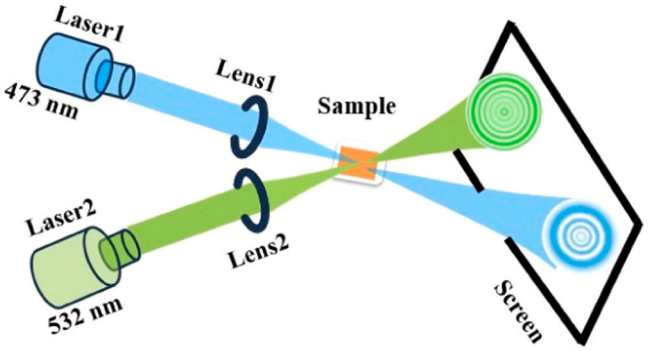

Fig. 2. AOS experimental set-up.

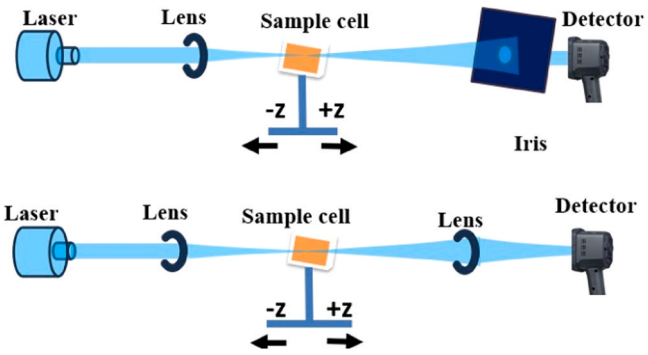

Fig. 3. Z-scan experimental set-up (a) CA and (b) OA.

3. Results

3.1. Experimental results

In order to create a curcumin analogue (cur-oxohexa), chloroacetylaceton was condensed with the aromatic aldehyde, Fig. 4. Utilizing spectroscopic methods, the hypothesized structures have been verified; adequate spectroscopic studies for the postulated structures were obtained for both compounds. The spectroscopic information of the produced compounds is described in this section.

3.1.1. IR spectrum of cur- oxohexa

The functional group bands were located in the anticipated locations, according to the IR spectra of the produced curcumin analogue. The spectrum of cur-oxohexa's (Supplementary material Fig. S1) displayed large bands at 3456 cm^{-1} that are ascribed to the enolic form and weak bands at 3047 and (2978–2877) cm^{-1} that are assigned to aromatic and aliphatic C-H, respectively. At (1695), (1583), and (1288) cm^{-1}, strong bands were discovered for the stretching vibrations of the C═O, C═C, and C-O groups, respectively.

3.1.2. Mass spectrum of compound cur-oxohexa

The molecular ion and the base peak were identified using the mass spectrum (Supplementary material Fig. S2) of the studied compound cur-oxohexa. Peak intensity data can be used to determine the stability of the fragment. In addition, the molecular ion [M+] and the primary fragmentation direction that followed from rupturing chelating the group's bonds with the methylene

and carbonyl groups were displayed in the mass spectrum (Fig. S2) of the produced cur-oxohexa molecule, the fragmentation scheme (Supplementary _material Fig. S3), as shown by the cleaving of the bonds at various points and the establishment of new bonds, further fragments were obtained [52,53].

3.1.3. ^{1}H and ^{13}C NMR spectra

The ^{1}H NMR spectrum is shown in (Supplementary _material Fig. S4) for curcumin analogue (cur-oxohexa) in DMSO-d6 at 25 °C the proposed structure. The protons in the -OCH_2CH_2O- group are responsible for the doublet-doublet signal that was visible in the spectrum at about 4.30 ppm. With a coupling constant of 8 ppm, two doublet signals from olefinic protons are seen at 6.94 and 8.25 ppm. doublet and doublet signals with J= 4 at 7.78 and 7.86 ppm are attributed to aromatic protons, as well as singlet signal at 7.52 ppm, also attributed to the aromatic protons. The ^{13}C NMR spectrum of the studied compound (Supplementary _material Fig. S5) displayed the carbon signal from the (C═O) were seen at (183.5) ppm. The spectrum also showed signals within the range of

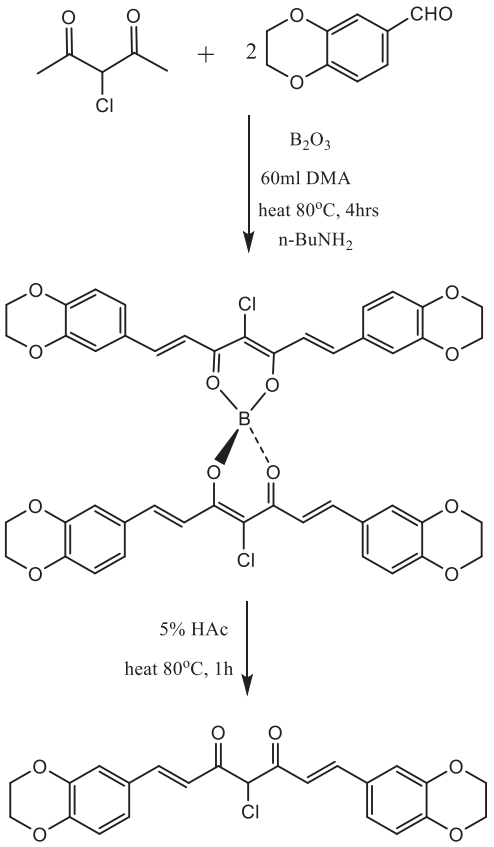

Fig. 4. Synthesis scheme of cur-oxohexa compound.

(144.8–120.5) ppm due to aromatic carbons as well as olefinic carbon, C-Cl carbon signal was detected at 73.1 ppm, while CH_2-CH_2 carbon signal was detected at 64.4 ppm. The results of ^{1}H and ^{13}C NMR spectra confirmed the expected structure of the cur-oxohexa.

3.1.4. Computational results

All theoretical calculations were carried out using the 6–311+G(d) basis set and the B3LYP methodology. The structures optimization and atomic labeling for both compounds are displayed in Fig. 5. The graphic displays geometrical optimization results showing the compound is nonplanar. The frequency and optimized data were computed with B3LYP/6–311+G(d) basis sets.

3.1.5. Quantum chemical descriptors (QCDs) and electronic properties (EP)

Each compound's chemical stability and reactivity are assessed using its HOMO, LUMO and molecular frontier orbitals (MFOs) [54]. The gap energy E distinguishes between HOMO and LUMO, where a large or smaller value indicates efficiency and has been used in nonlinear optics. The HOMO is tied to the capacity to donate an electron, while the LUMO is related to the ability to take an electron [55,56].

We were able to acquire the isodensity plots, which depict the distributions of HOMO and LUMO electron clouds of the enol-form and keto-form for curcumin analogue, in order to understand the mechanism of the transfer of charge from HOMO to LUMO, Fig. 6. HOMO typically localizes on the group of donor phenyl, but LUMO is on the middle 1,3-dike to the acceptor group, as can be seen from

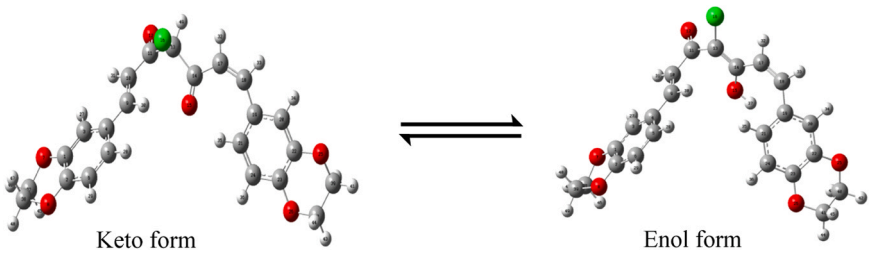

Fig. 5. The optimized 3D structures of synthesized cur-oxohexa compound.

here. Using B3LYP/6311+ G (d) level calculations, the E_{HOMO}-E_{LUMO} gap energy for the curcumin molecule depicts the chemical activity of the compound. The ability to acquire an electron is represented by LUMO as an electron acceptor, while HOMO stands for the capacity to give an electron. The values of HOMO energy and LUMO energies for cur-enol- oxohexa's and keto-forms were discovered to be −5.89 and −2.18 eV and −6.04 and −2.51 eV, respectively. E_{HOMO}-E_{LUMO} gaps energy are smaller for the enol and keto forms, at 3.71 and 3.546 eV, respectively. Electron donor and acceptor groups control the charge transfer from HOMO to LUMO, which is what causes the 3rd-order NLO response or the second-order hyperpolarizability [57].

Based on our knowledge of the importance of NLO features presented in past studies [58–61], we have evaluated the NLO characteristics of synthesized compound and have looked at their NLO characteristics. Numerous QCDs have been produced to analyze the NLO properties on a theoretical basis. The growing NLO features are given by increases in the values of E_{HOMO}, So, and S. The NLO characteristics likewise deteriorate as E_{LUMO}, IE, and η. Cur-oxohexa, the newly synthesized compound, exhibits greater values for E_{HOMO}, S, and S_o than for LUMO energy, gap of energy, and IE, indicating that they have superior NLO characteristics. The QCDs, Table 1, and, Table 2, findings demonstrate the closeness of the values between synthetic analogues and natural curcumin dye. Additionally, it demonstrates that they exhibit NLO characteristics similar to curcumin dye.

3.1.6. Vibrational spectrum (IR analysis)

In order to compare actual and theoretical IR data and to better comprehend the connection between wavenumber and molecule structure, calculations of theoretical frequencies were made and documented. To ascertain the link between the IR values in theory and experiment (Supplementary-material Fig. S6), estimated values are compared to the experimental data. It is clear that the calculated frequencies closely match the frequencies of the most significant bands in the actual spectra, whereas the variations in band intensities resulting from the neglect of intermolecular interactions. The B3LYP technique with the 6–311+G (d) basis set was used to calculate the IR wavenumber for each group in the compound. Fig. 7 displays the statistical properties of the estimated IR wavenumber and the experimental proof of the molecule cur-oxohexa. As is evident, the outcomes are reasonably consistent with the experimental values.

3.1.7. Analysis of the population of Mulliken

Calculations of Mulliken atomic charge are crucial for applying quantum chemistry calculations to molecule systems since atomic charges influence properties such as the dipole moment and molecules polarized. The compound cur- oxohexa, which were made using

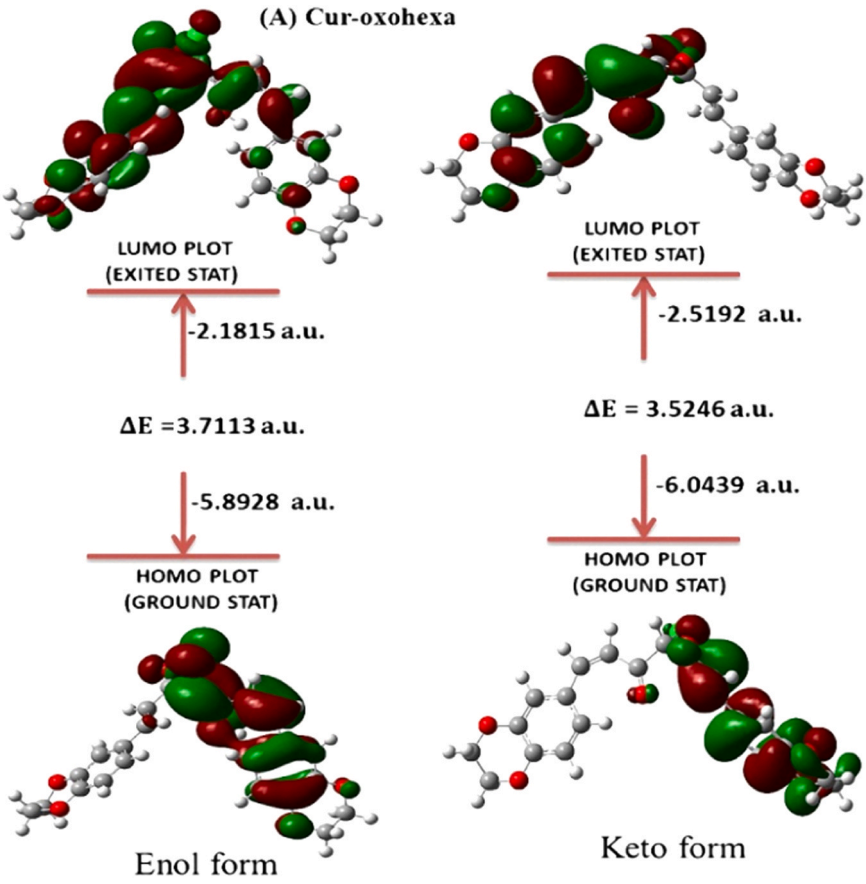

Fig. 6. The atomic orbital compositions for the curcumin analogue frontier molecular orbitals of cur-oxohexa using DFT/ B3LYP 6–311+G(d).

Table 1
The Enol and keto thermodynamic properties at 298.15 K in ground state, calculated by DFT/B3LYB 6–311+G(d) for cur-oxohexa.

Parameters	Units	Enol form	keto form
Zero point vib. Energy	Kcal/mol	-1799.31966	-1799.33912
Entropy (S)	cal. mol^{-1} k^{-1}	186.823	186.985
Electronic Energy (EE)	Hartree	-1799.69495	-1799.7155
Heat Capacity (Cv)	Cal/mol.K	100.633	99.095

Table 2
Some NLO properties QCDs of calculated for cur-oxohexa.

Parameters	Unit	Natural Curcumin dye	Enol-form	Keto-form
E_{HOMO}	eV	-5.72	-5.892	-6.043
E_{LUMO}	eV	-2.51	-2.181	-2.519
ΔE	$(kJ.mol^{-1})$	3.21	3.711	3.546
EA	eV	2.51	2.181	2.519
IE	eV	5.72	5.892	6.043
η	eV	1.605	1.855	1.773
S	$(eV)^{-1}$	0.623	0.538	0.564
S_o	eV	0.311	0.269	0.282
χ	eV	4.115	4.037	4.281
Cp	eV	- 4.115	- 4.037	- 4.281
ω	eV	5.275	4.391	5.169
ΔN_{max}	eV	2.563	2.594	2.414
μ	eV	- 4.115	- 4.037	- 4.281

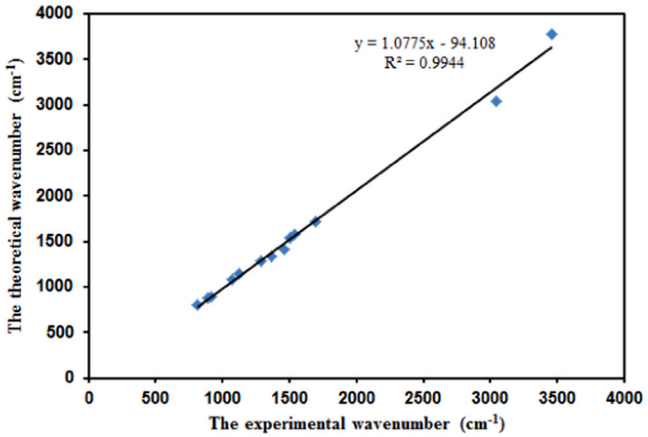

Fig. 7. Experimental values versus theoretical ones for infrared of cur-oxohexa.

the Mulliken population, are shown by their atomic charges in Fig. 8. ulliken atomic charges for cur-oxohexa demonstrated that the positive charges on the C1, C2, C22, and C23 atoms in the aromatic rings (two sides) and on the C37-C40 atoms between oxygen atoms result from the presence of electronegative oxygen atoms. The other atoms (O7, O8, O25, O26) are all negative as one would anticipate.

offer a ballpark estimate for the actual application of the produced substances as possible medications. Any substance is said to have low toxicity, excellent absorption, and oral bioavailability if it has two or fewer breaches of Lipinski's rule of five. All synthetic compounds have low toxicity, good oral bioavailability, and good absorption, according to the drug likeness check of the compounds (Fig. 9). These chemicals consistently adhere to the rule of five. (Supplementary material Fig. S6) all results of AMDE were created using the Swiss ADME program and gathered in Table S1 (Supplementary material).

3.1.8. Electronic absorption spectrum of cur-oxohexa

The electronic absorption spectra of cur-oxohexa compound in ethanol or chloroform are shown in Fig. 10. Each spectrum exhibited three bands, by using ethanol or chloroform as a solvent, (240, 278, 452 nm) and (236, 264, 456 nm) respectively. In general, the spectrum of electronic transition of a curcumin compound in solution shows two bands: one band occurs in the ultraviolet region and is related to the electronic π-π* transition of the feruloyl acetone, while the other band is the aromatic ring's electronic transition band in the visible region. The second band, which is a part of the electronic π-π* transition of delocalization of all curcumin compounds [62, 63], is visible in the visible region. The compound under study exhibits three bands in its spectrum where ethanol is used as a solvent,

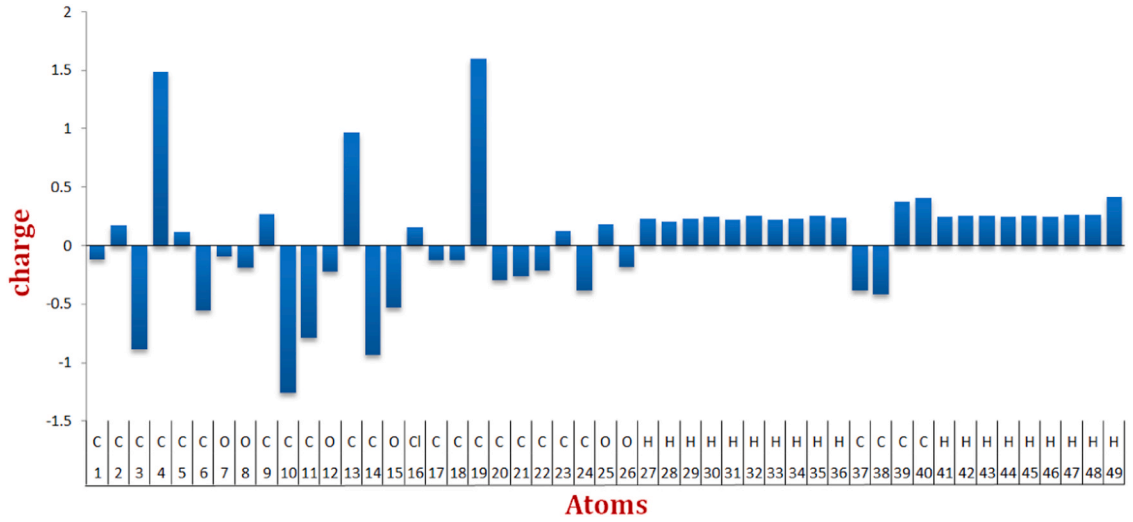

Fig. 8. The distribution of atomic charge for studied compounds according to Mulliken.

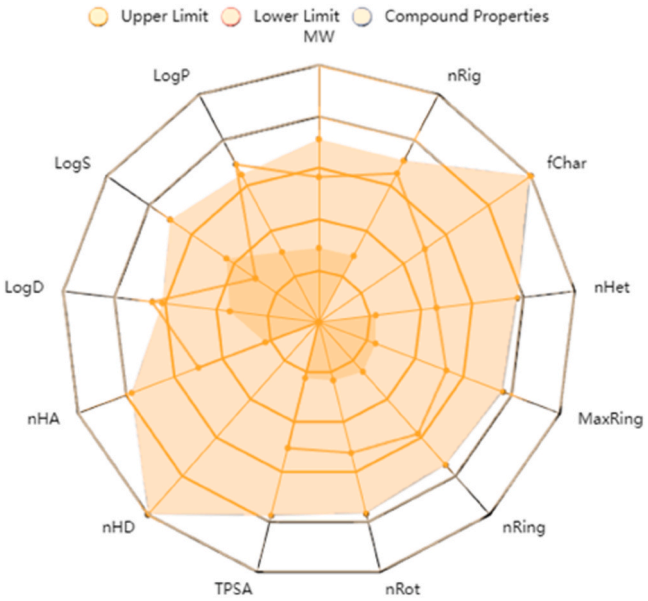

Fig. 9. Bioavailability Radar and the physicochemical characteristics of the substance under study.

as seen in Fig. 10. A band with a shorter wavelength, which is attributed to the aromatic moiety's π-π*, manifests in the UV area at 240 nm with ε of 11610 cm^2 mol^{-1}. The half molecule (feruloyl acetone) was identified as the source of the remaining band at 278 nm. The whole molecule was identified as the source of the other

band at 452 nm, which has a molar absorptivity of 8480 cm^2 mol^{-1}. Three bands are seen in the spectrum of cur-oxo-hexa solution in chloroform as a solvent. The first band, at 236 nm in the UV region with ε = 26300 cm^2 mol^{-1}, has a shorter wavelength and is thought to be attributed to π-π* of aromatic rings. The other two bands are located at 264 nm with ε =10250 cm^2 mol^{-1} and 456 nm with ε = 7300 cm^2 mol^{-1} attributed to the half molecule and the whole molecule respectively.

3.1.9. The theoretical spectra of electronic absorption the cur-oxo-hexa compound

Using the TD-SCF approach on the CAM-B3LYP/6–311 G(d,p) level of theory, the singlet excited state in ethanol and chloroform was computed in order to explain the electronic spectrum nature of the examined chemical. Cur-oxo-hexa molecule in ethanol was projected to consist of three bands, which occurred at 400.8, 278.6, and 232.8 nm. The oscillator strength, *f*, for these bands were 2.6896, 0.1436, and 0.3532, respectively, as indicated in Table 3. Three bands make up the electrical absorption calculation findings of the cur-oxo-hexa molecule in ethanol. The pure transition from HOMO to LUMO, which is associated with intramolecular charge

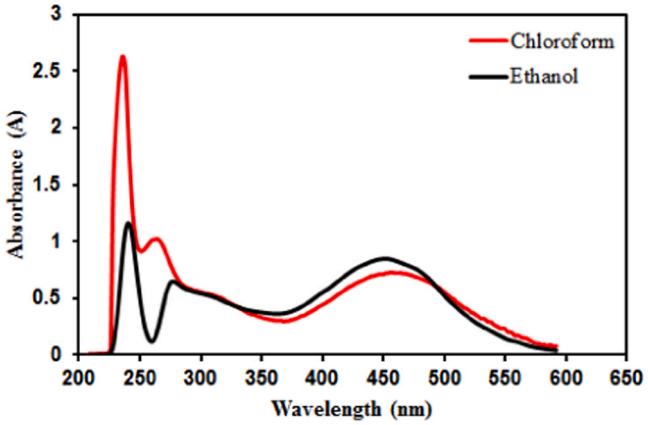

Fig. 10. The electronic spectrum of cur-oxohexa in the chloroform and ethanol.

transfer (ICT), is one of the three transitions indicated by the absorption band with a larger wavelength and oscillator intensity [64]. With oscillator strength of 0.1436, the second band at 278.4 nm is made up of the electronic transitions shown in Table 3, including. Ultimately, the transitions shown in Table 3 result in the band having greater energy. Three bands are also the consequence of the electrical absorption of the cur-oxo-hexa molecule in chloroform. One of the three transitions to which the absorption band with a greater wavelength and oscillator intensity belongs is the pure transition from HOMO to LUMO, which is also ascribed to the (ICT). With an oscillator strength of 0.1330, the second band at 278.4 nm is made up of a series of electronic transitions, such as those given in Table 3.

3.1.10. Linear absorption coefficient

Using Fig. 10 and the equation referred to in [65], cur-oxohexa absorption coefficient in the ethanol is calculated at the wavelengths 473 nm and 532 and found equal to 17.98 and 5.68 cm^{-1}, respectively.

Table 3
Band maxima, both theoretical and practical, and intensities of the cur-oxohexa molecule are using CAM-B3LYP/6–311 G(d,p).

Solvent	Major Transitions	Transition probability	Transition probability percent	Theoretical λ_{max} (nm)	Experimental λ_{max} (nm)	Oscillator strenght	Experimental oscillator strength ($cm^2.Mol^{-1}$)
Ethanol	H-2 → L	0.1575	4.96%	400.8	452	2.6896	8480
	H-1 → L+1	0.1565	4.58%				
	H → L	0.6567	86.25%				
	H-7 → L	0.1065	2.26%	278.6	278	0.1436	6460
	H-4 → L	0.5843	68.28%				
	H-3 → L+1	0.2509	12.59%				
	H-2 → L	0.1548	4.79%				
	H-1 → L+2	-0.1415	4.0%				
	H → L+3	0.1447	4.18%				
	H-7 → L	-0.1176	2.76%	232.8	240	0.3532	11610
	H-6 → L+1	-0.1011	2.04%				
	H-2 → L	0.2467	12.17%				
	H-2 → L+4	0.1158	2.68%				
	H-1 → L+1	0.3951	31.22%				
	H → L	-0.1616	10.09%				
	H → L+3	-0.3117	19.43%				
Chloroform	H-1 → L	0.1603	5.13%	439.9	456	2.0514	7300
	H → L+1	0.1641	5.38%				
	H → L	0.6557	85.98%				
	H-4 → L	0.5662	64.11%	278.4	264	0.1330	10250
	H-3 → L+1	0.2755	15.18%				
	H-2 → L	0.1260	3.17%				
	H-1 → L+2	-0.1688	5.69%				
	H → L+3	-0.1715	5.88%				
	H-2 → L	0.2053	8.42%	233.4	236	0.2150	26300
	H-2 → L+4	-0.1002	2.00%				
	H-1 → L+1	0.5596	62.63%				
	H-1 → L+2	0.1171	2.74%				
	H → L	0.1471	4.32%				
	H → L+3	0.1826	6.66%				

3.2. Nonlinear studies

Fig. 11 shows the changes in the diffraction patterns with different laser beam power input, which varied gradually from zero to 56 mW where it is seen that as the power input increased, the rings number in the pattern increased. Since the amount of energy absorbed by the medium increased with the increase in power input so that the amount of heat generated in the medium spatially increase in the three dimension and the divergent lens generated focal length increase so that the area of the beam increased i.e., the DPs area increased. Also, the patterns area increased up to a specific power input, each pattern is symmetric in the x-y plane, where the vertical thermal current exceeds the horizontal thermal current. The vertical motion of heat act on the replacement of the upper hot part of the medium by a cold one that reduces the refractive index so that the phase change of the beam in the upper part reduced hence the radii of the rings in the upper part reduced so that the DPs appears compressed then the upper half start to increase in small ratio compare to the lower half i.e. beam propagation suffers self-induced (deformation) as the power increases and starts to form ring patterns with squeezed shapes. Each ring diameter in the upper half grew less than the lower half as a result of the vertical thermal convection current that moves the warm layer upward and replaces it with a cold one so the refraction index change in the upper part is smaller than the lower part so does the change in phase suffered by the beam. Fig. 12 shows the effect of the laser beam wave front type on the type of DP. It can be seen that the DP type depends on the beam wave front type. As the laser beam falls on the positive lens, the wave front varies in the same way shown in Fig. 13, so that the radius (R) of the wave front sign switches from +R, to –R, as it passes through the positive lens, such an effect was noticed experimentally and proved theoretically by a number of researchers as early as 1984 it is believed that the type of interaction of the laser beam with nonlinear medium depends on the wave front type, this is why two DPs types resulted [43–45]. Fig. 14 shows the temporal evolution of chosen DP at a power input of 56 mW. It started with a bright spot at the initial time, then the area of the spot increased as time lapsed, an indication of the evolution of the effect of SDF up to a certain time, ring appeared whose number and area increased and then the upper half of the pattern shrink, an indication of losing symmetry due to the increase of thermal verities convection current vertically exceeding the thermal horizontal conduction current [66].

Fig. 15 shows the illustration diagram of the experimental installation of the AOS. One signal at the wavelength of 473 nm, which we call the controlling beam, where the sample has a large absorption coefficient of 17.98 cm^{-1} and another beam of wavelength 532 nm called the controlled, and the medium have an absorption coefficient of 5.68 cm^{-1}. Both beams are of cw character. When the controlled beam passes the medium alone, no rings appear alone when the power input varied in the range of 0–50 mW as shown in Fig. 15 a(i). When the controlling beam pass through the medium ring patterns appear where its power accedes a certain threshold as shown in Fig. 15a(iii). When both beams pass through the medium, two DPs type resulted, one due to spatial self-phase modulation (SSPM) of the 473 nm beam and one due to cross self-phase modulation (XSPM) [46–48] as shown in Fig. 15a(ii and iii). In the present of both beams, the controlling beam affects its own DPs area, number of rings, the intensity and the asymmetry as shown in Fig. 15b (i-iii) at the same time it affect the controlled beam DPs via it's area, number of rings and asymmetry but not it's intensity as shown in Fig. 15c (i-iii). The controlled beam does not affect the controlling beam DPs but it affects its own DPs intensity only as shown in Fig. 15d (i-iii). The 473 nm and 532 nm beams DPs are of cw character. When changing the output power of the controlling beam to pulse (square one) via the connection of the 473 nm laser device to a TTL function of a frequency generator so that its output became pulsed and keeping the output power of the controlled, 532 nm, beam cw and let both beams to pass through the medium, Fig. 16 shows the result of passing both beams, two types of DPs generated. The pulse controlling 473 nm beam forces the controlled 532 nm beam DPs to become pulsed one too.

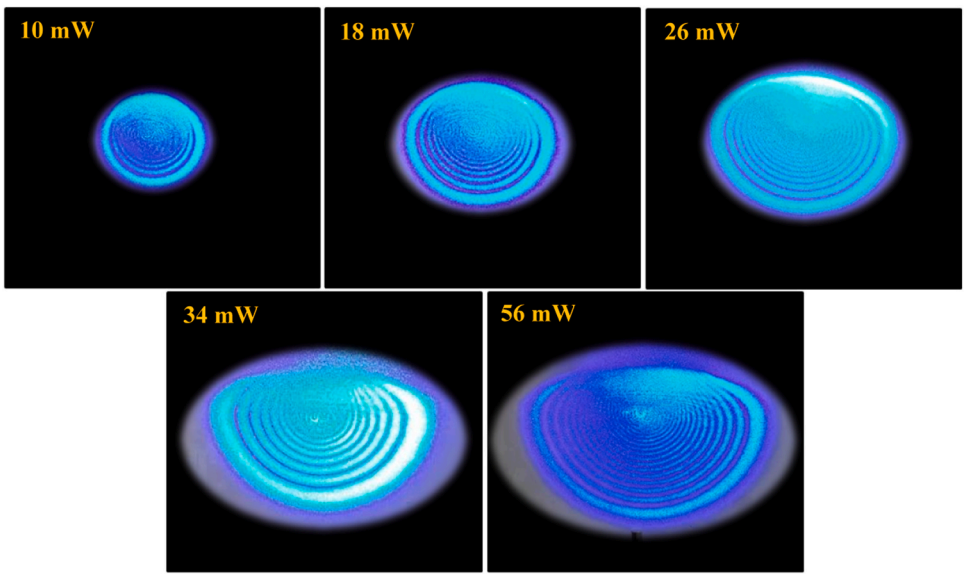

Fig. 11. Typical DPs: variation with the power input increase of laser light beam in cur-oxohexa.

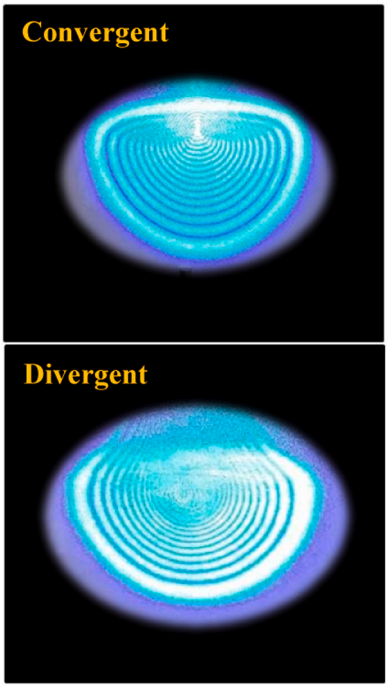

Fig. 12. Typical DPs: dependence on the wave front of laser beam in cur-oxohexa input power 56 mW.

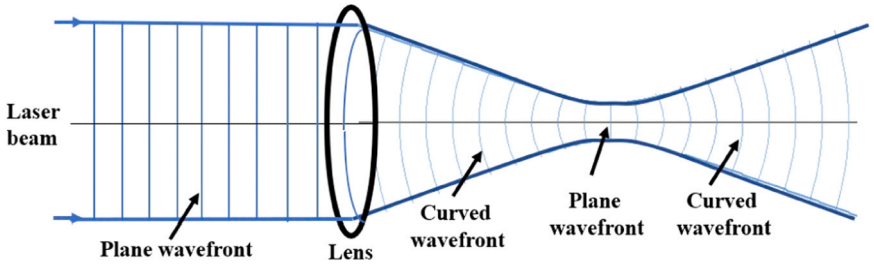

Fig. 13. Variation of plane wave laser beam wave front as it pass through a positive lens.

The result of performing the CA Z-scan on the sample is reported in Fig. 17a. The incident intensity used in these measurements is 688.2 W/cm^2 that corresponds to a power input of 4 mW. The curve in Fig. 17a showed a peak-valley configuration (negative INLR), in other words, the effect of SDF. The result that we obtained from conducting the OA Z-scan on the sample is shown in Fig. 17b. The Figure reveals that absorption saturation has occurred at z = 0. Fig. 17c represents the result of dividing the Fig. 17a by b. The seeking for pure refractive index effect required division process. The continuous wave laser beam use led to thermal nonlinearity.

3.3. Calculation of the INLR

3.3.1. Due to DP

To estimate the induced refraction index changes, Δn, and the magnitude of the INLR, n_2, of the curcumin analogues based on the experimental data of the DPs such as the total number of rings, incident light wavelength, cell thickness, d, the input power are used. For a Gaussian beam traversing the sample cell, the transmitted light at the sample exit plane cell is cylindrical, so that the phase shift, $\Delta\varphi(r)$, is expressed as follows [1]

$$\Delta\varphi(r) = \Delta n \exp\left(-\frac{2r^2}{\omega^2}\right) kd \tag{1}$$

$$\Delta\varphi(r) = \Delta\varphi_o \exp\left(-\frac{2r^2}{\omega^2}\right) \tag{2}$$

$\Delta\varphi_o$ is the laser beam on axis phase shift, r is the distance away from the beam axis, ω is radius of the laser beam, and $k = 2\pi/\lambda$ is the

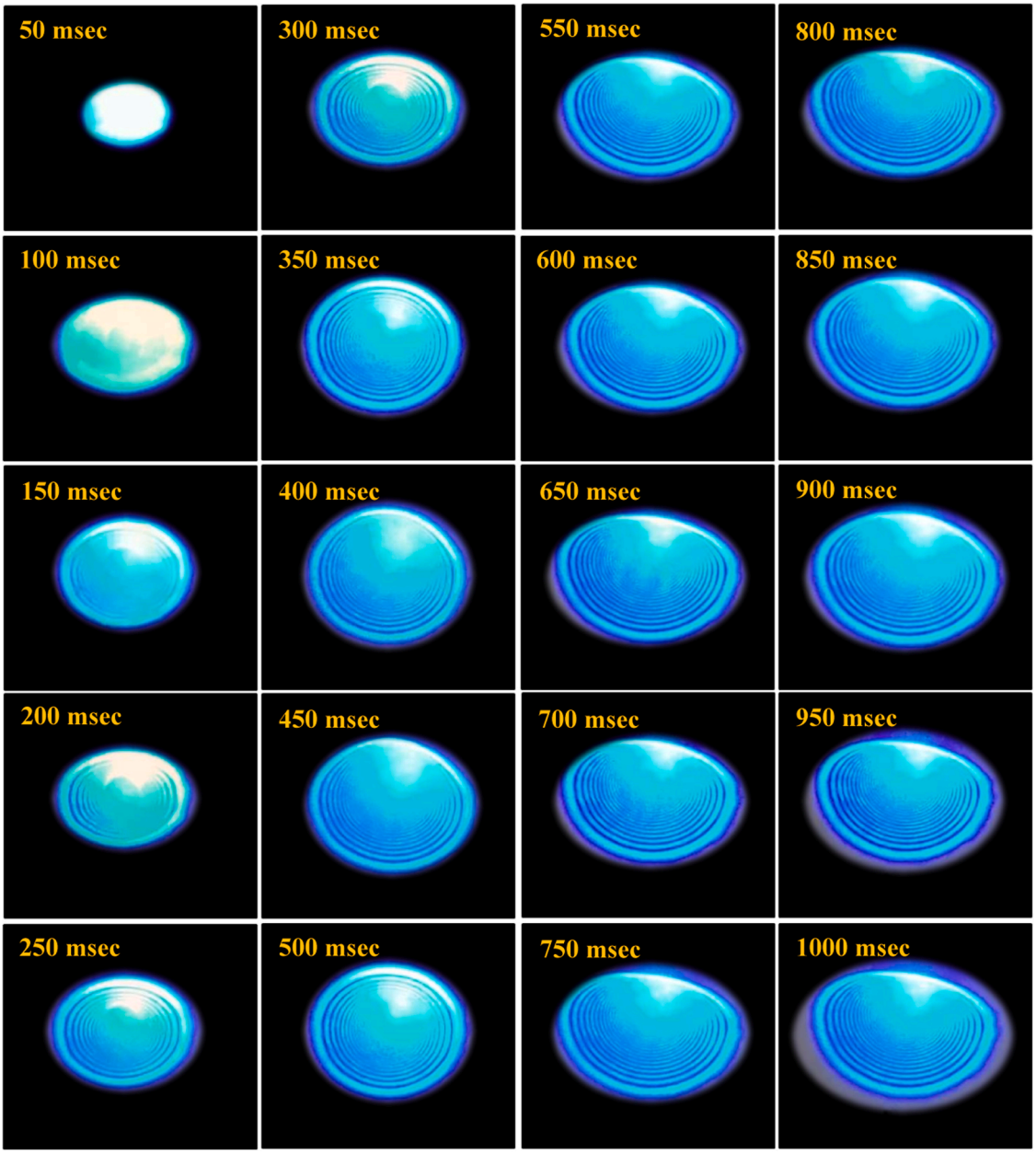

Fig. 14. Typical DPs: temporal evolution at laser beam input in cur-oxohexa.

beam wave vector (λ is the laser beam wavelength) so that

$$\Delta\varphi_o = (\Delta \mathrm{n} \mathrm{d})\mathrm{k} \tag{3}$$

$\Delta\varphi_o$ is related to maximum number of rings, N, at the maximum input power i.e.,

$$\Delta\varphi_o = 2\pi \mathrm{N} \tag{4}$$

So that

$$\Delta \mathrm{n} = \frac{\mathrm{N}\lambda}{\mathrm{d}} \tag{5}$$

λ is the beam wavelength.n_2 and Δn are related to the laser beam intensity, I, as follows

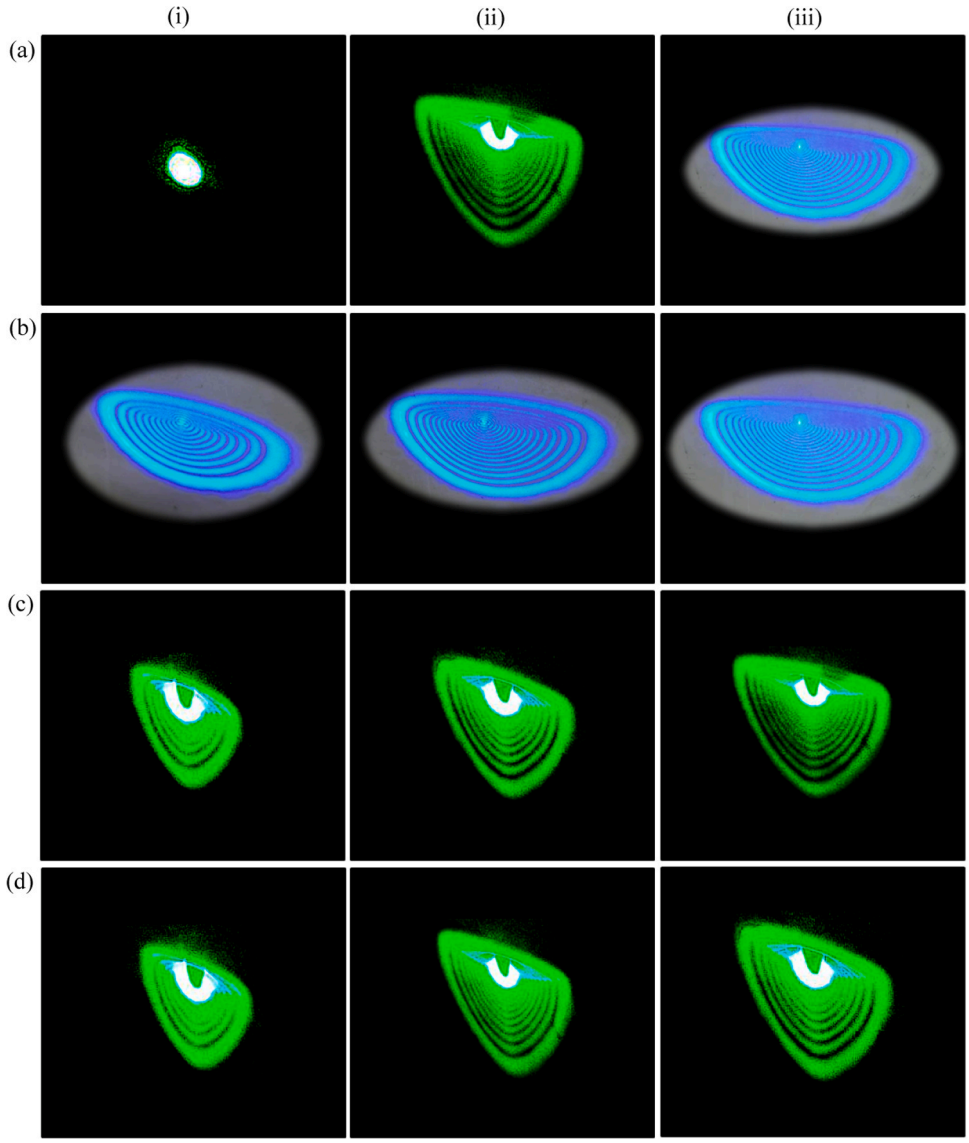

Fig. 15. Static cw AOS using two laser beams, in cur-oxohexa.

$$n_2 = \frac{\Delta n}{I} \tag{6}$$

$$I = \frac{2P}{\pi\omega^2} \tag{7}$$

P is the laser beam power input, $\lambda = 473$ nm, $d = 0.1$ cm, and $\omega = 19.235$ μm, the INLR, n_2 and Δn were calculated for different input powers and the results obtained are given in Table 4.

3.3.2. Z-scan

The INLR, n_2, and CNLA,β, are given by the following formulas [6,7]

$$n_2 = \frac{\Delta\varphi\lambda}{2\pi L_{eff} I} \tag{8}$$

$$\beta = \frac{2\sqrt{2}\Delta T}{L_{eff} I} \tag{9}$$

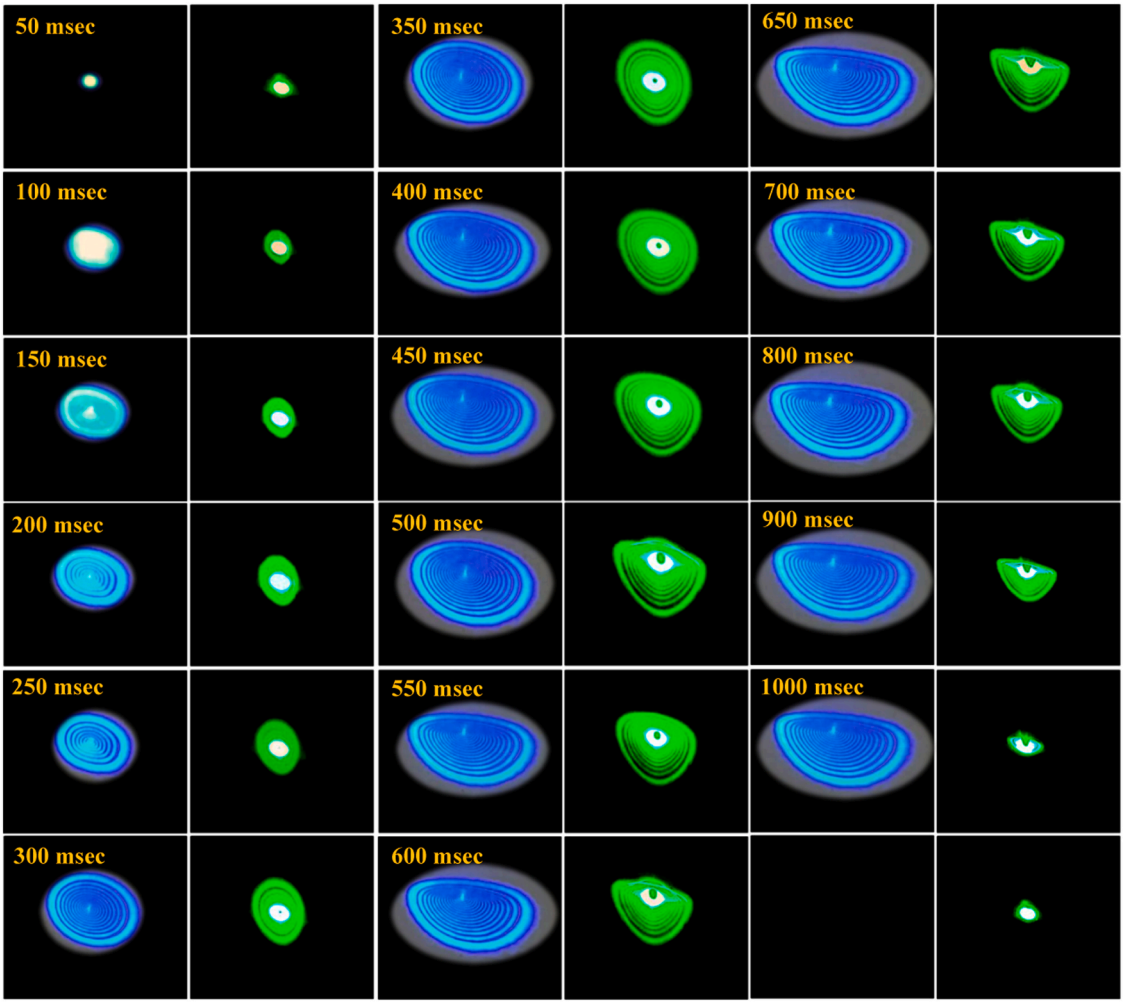

Fig. 16. Temporal evolution of the pulsed controlling beam DPs lead to temporal DPs of the cw controlled beam. Such behavior is called dynamic AOS in cur-oxohexa.

$$L_{eff} = \frac{1 - \exp(-\alpha d)}{\alpha} \tag{10}$$

$$\Delta\varphi_o = \frac{\Delta T_{p-v}}{0.406(1-S)^{0.25}} \tag{11}$$

$$\Delta T_{p-v} = T_p - T_v \tag{12}$$

$$\Delta T = 1 - T_p \tag{13}$$

Where L_{eff} is the sample effective thickness, S is linear transmittance of aperture, T_p and T_v represent the peak transmittance and valley transmittance, respectively. By finding the values of ΔT_{p-v} and ΔT from Fig. 17a and c and using Eqs. 8 - 13, we determined the value of the INLR and NLAC of the compound and found them to be 3.58×10^{-11} m^2/W and 2.23×10^{-3} cm/W respectively. The value of the INLR calculated for the cur-oxohexa using the Z-scan is larger than its value for the compounds referred to in studies [67–74], which proves that the cur-oxohexa can be a candidate for use in optical devices.

4. Conclusion

We synthesized a novel curcumin analogue dye and calculated its index of nonlinear refraction (INLR) under irradiation with a 473 nm laser beam that led to the generation of diffraction patterns (DPs) and the Z-scan technique. The sample coefficient of nonlinear absorption (CNLA) is calculated due to the second technique. The study of all-optical switching (AOS) led to the fact that

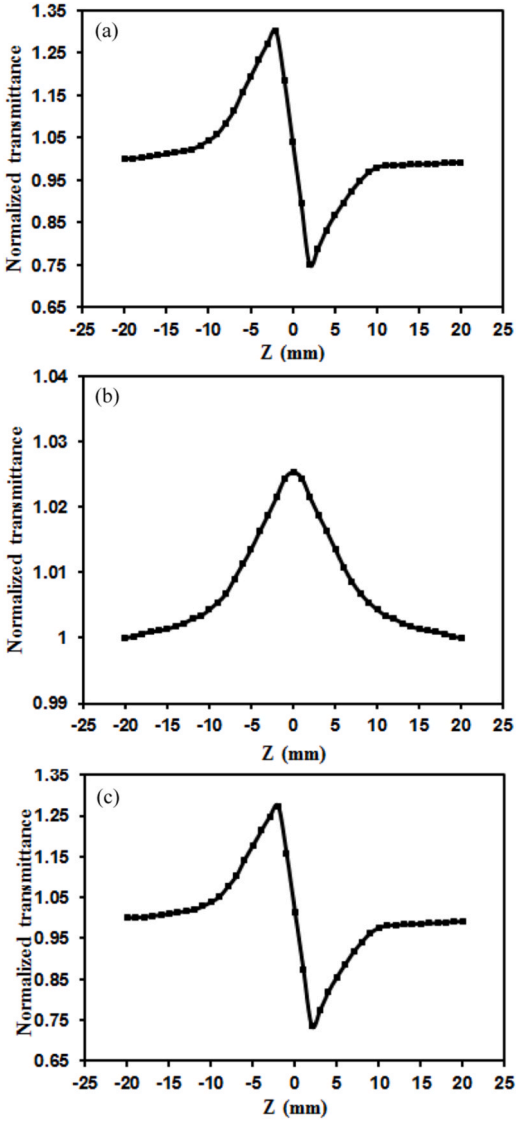

Fig. 17. Z-scan data for power input of 4 mW: (a) CA, (b) OA, Z-scans. (c) the division of (a) over (b), in cur-oxohexa.

Table 4
Nonlinear refractive index and refraction index change calculated by the DPs.

P(mW)	N	$\Delta n \times 10^{-3}$	$n_2 \times 10^{-11}$ m^2/W
10	2	0.94	5.12
18	4	1.89	5.73
26	6	2.83	5.91
34	9	4.25	6.78
56	15	7.09	6.86

such material is able to show two types of AOS, viz., static AOS and dynamic AOS.

CRediT authorship contribution statement

Kawkab Ali Hussein: Software, Investigation. **Qusay M. A. Hassan:** Writing – original draft, Methodology, Investigation, Formal analysis. **Ayman G. Faisal:** Methodology, Investigation, Formal analysis, Data curation. **Tahseen A. Alsalim:** Writing – original draft, Software, Investigation, Formal analysis. **H. A. Sultan:** Software, Methodology, Investigation. **Fadhil S. Kamounah:** Resources,

Methodology, Investigation, Formal analysis. **C. A. Emshary:** Writing – review & editing, Resources, Methodology, Investigation, Formal analysis, Data curation.

Declaration of Competing Interest

The authors declare that they have no known competing financial interests or personal relationships that could have appeared to influence the work reported in this paper.

Data Availability

No data was used for the research described in the article.

Appendix A. Supporting information

Supplementary data associated with this article can be found in the online version at doi:10.1016/j.ijleo.2024.171800.

References

[1] K. Ogusu, Y. Kohtani, H. Shao, Laser-induced diffraction rings from an absorbing solution, Opt. Rev. 3 (1996) 232–234.
[2] Kh.A. Al-Timimy, Qusay M.A. Hassan, H.A. Sultan, C.A. Emshary, Solvents effect on the optical nonlinear properties of the sudan iv, Optik 224 (2020), 165398 (15 pp).
[3] Ahmed S. Al-Asadi, Qusay M.A. Hassan, Amjad F. Abdulkader, H. Bakr, C.A. Emshary, Enhancement of the linear, nonlinear and optical limiting properties of epoxy resin decorated by zinc oxide nanoparticles, Phys. Scr. 95 (2020), 085503(12pp).
[4] Qusay M.A. Hassan, H.A. Sultan, Ahmed S. Al-Asadi, Ayat Jawdat Kadhim, Nazar A. Hussein, C.A. Emshary, Synthesis, characterization, and study of the nonlinear optical properties of two new organic compounds, Synth. Met. 257 (2019), 116158(14 pp).
[5] Dakhil Zughayir Mutlaq, Qusay M.A. Hassan, H.A. Sultan, C.A. Emshary, The optical nonlinear properties of a new synthesized azo-nitrone compound, Opt. Mater. 113 (2021), 110815(13 pp).
[6] M. Sheik-Bahae, A.A. Said, E.W. Van Stryland, High sensitivity single beam n_2 measurements, Opt. Lett. 14 (1989) 955–957.
[7] M. Sheik-Bahae, A.A. Said, T. Wei, D.J. Hagan, E.W. Van Stryland, Sensitive measurement of optical nonlinearities using a single beam, IEEE J. Quant. Electron. 26 (1990) 760–769.
[8] R.R. Mallah, D.R. Mohbiya, M.C. Sreenath, S. Chitrambalam, I.H. Joe, N. Sekar, Fluorescent meso- benzyl curcuminoid boron complex: Synthesis, photophysics, DFT and NLO study, Opt. Mater. 84 (2018) 786–794.
[9] X. Hu, P. Jiang, C. Ding, H. Yang, Q. Gong, Picosecond and low-power all-optical switching based on an organic photonic-bandgap microcavity, Nat. Photo 2 (2008) 185–189.
[10] U.J. Al-Hamdani, Qusay M.A. Hassan, A.M. Zaidanc, H.A. Sultan, K. Ali Hussain, C.A. Emshary, Z.T.Y. Alabdullah, Optical nonlinear properties and all optical switching in a synthesized liquid crystal, J. Mol. Liq. 361 (2022) 119676.
[11] A.M. Dhumad, Qusay M.A. Hassan, T. Fahad, C.A. Emshary b, N.A. Raheem, H.A. Sultan, Synthesis, structural characterization and optical nonlinear properties of two azo- β-diketones, J. Mol. Struc. 1235 (2021) 130196.
[12] S. Srivastava, P. Gupta, Amandeep, R.P. Singh, Synthesis of 4-((1E, 6E)-7-(4-hydroxy-3-methoxyphenyl)-3, 5-dioxohepta-1, 6- dienyl)-2-methoxyphenyl 4-fluorobenzoate, a novel monoester derivative of curcumin, its experimental and theoretical (DFT) studies, J. Molecu. Struc. 1109 (2016) 58–66.
[13] M. Asghari-Khiavi, P. Hojati-Talemi, F. Safinejad, Polarizability and first-order hyperpolarizability of cyclic imides, J. Mol. Struct. Theochem. 910 (2009) 56–60.
[14] A. Saeed, Qusay M.A. Hassan, C.A. Emshary, H.A. Sultan, R.S. Elias, The nonlinear optical properties of two dihydropyridones derived from curcumin, Spectrochim. Acta Part A: Molecu. BioMol. Spectros. 240 (2020) 118622.
[15] M.R.S.A. Janjua, A. Mahmood, M.F. Nazar, Z. Yang, S. Pan, Electronic absorption spectra and nonlinear optical properties of ruthenium acetylide complexes: a dft study toward the designing of new high NLO response compounds, Acta Chim. Slov. 61 (2014) 382–390.
[16] N. Islam, S.S. Chimni, DFT investigation on nonlinear optical (NLO) properties of novel borazine derivatives, Comput. Theor. Chem. 1086 (2016) 58–66.
[17] B. Aggarwal, I.D. Bhatt, H. Mtchikawa, K.S. Ahn, G. Sethi, S.K. Sandur, C. Sundaram, N. Seeram, S. Shishodia, Tarmeric, Genus curcuma, Ch 10 (2006) 297–302.
[18] F. Payton, P. Sandusky, W.L. Alworth, NMR study of the solution structure of curcumin, J. Nat. Prod. 70 (2007) 143–146.
[19] Y. Erez, I. Presiado, R. Gepshtein, D. Huppert, Temperature dependence of the fluorescence properties of curcumin, J. Phys. Chem. A 115 (2011) 10962–10971.
[20] S. Ansari, S. Tilani, H. Abbai, M. Siraj, A. Hashimi, Y. Ahmed, R. Khatoon, A.H. Rifas, Curcuma longa:Treasure of medicinal properties, Celled 10 (2010) 1–7.
[21] R.S. Elias, B.A. Saeed, K.Y. Saour, N.A. Al-Maoudi, Microwave –assisted synthesis of dihydropyridane from curcumin, Tetrah. Lett. 49 (2008) 3049–3051.
[22] R.S. Elias, Qusay M.A. Hassan, C.A. Emshary, H.A. Sultan, B.A. Sseed, Formation and temporal evolution of diffraction ring patterns in a newly prepared dihydropyridone, Spectrochic. Acta Part A:Mol. Biomol. Spect. 223 (2019), 117297(16pp).
[23] B.A. Saeed, W.A. Radhi, R.S. Elias, Synthesis novel 2,3-dihydro-4-pyridinanes from bisdemthoxyc-curcumin under microwave irradiation, Tetrah. Lett. 51 (2010) 5798–6800.
[24] K.E. Jasim, S. Cassidy, F.Z. Henari, A.A. Dakhel, Curcumin dye-sensitized solar cell, J. En. Pow. Eng. 11 (2017) 406–416.
[25] T. Ganesh, H. Kim, S.J. Yoon, B.H. Kil, N.N. Maldar, J.W. Han, S.-H. Han, Photoactive curcumin –derived dyes with surface anchoring moieties used in ZnO nanopartical-based dye-sensitized solar cell, Mat. Chem. Phys. 123 (2010) 62–66.
[26] K.I. Pripadasini, The chemistry of curcumin from extraction to therapentic agent, Molecules 19 (2014) 20091–20112.
[27] R.S. Elias, Qusay M.A. Hassan, H.A. Sultan, A.S. Al-Asadis, B.A. Saeed, C.A. Emshary, Thermal nonlinearities for three-curcuminoids, measured by diffraction ring patterns and Z-scan under visible CW laser illumination, Opt. Las. Technol. 107 (2018) 131–141.
[28] H.A. Sultan, Qusay M.A. Hassan, A.S. Al.Asadi, R.S. Elias, H. Bakr, B.A. Saeed, C.A. Emshary, Far filed diffraction patterns and optical limiting proprieties of bisedmethoxy curcumin solution under CW illumination, Opt. Mater. 85 (2018) 500–509.
[29] D. Patra, R. El-Kurdi, Crcumin as a novel reducing and stablilizing agent for the green synthesis of metallic nanoparticales, Gre. Chem. Lett. Rev. 14 (2021) 474–487.
[30] T.S. Yasagh, Synthesis and characterization of some polyester derived from curcumin, J. Thi-Qar Sci. 3 (2012) 141–148.
[31] H. Ligeret, S. Barthelemy, G.B. Doulakas, P.-A. Carrupt, J.-P. Tillement, S. Labidalle, D. Movin, Fluoride curcumin derivatives: new mitochondrial uncoupling agents, FEBS Lett. 569 (2004) 17–42.
[32] M. Balasubramanyam, A.A. Koteswari, R.S. Kumar, S.F. Monickaraj, J.U. Maheswar, V. Mohan, Curcumin-induced inhibition of cellular reactive oxygen species generation: novel therapeutic implications, J. Biosci. 28 (2003) 715–721.

[33] K.I. Priyadarsini, Photophysics, photochemistry and photobiology of curcumin: Studies from organic solutions, bio-mimetics and living cells, J. Photochem. Photobio. C:Photochem. Rev. 10 (2009) 81–95.
[34] S.-H. Kim, S.-Y. Gwon, S.M. Burkin Shaw, Y.A. Son, The photo- and electrophysical properties of curcumin in aqueous solution, Spectroch. Act. Part A:Mol. Biomol. Spectra 76 (2010) 384–387.
[35] F.Z. Henari, S. Cassidy, Nonlinear optical studies of curcumin metal derivatives with CW Laser, AIP Conf. Proc. 1653 (2015) 020044 (10 pp).
[36] J.L. Oudar, Hyperpolarizabilities of the nitroanilines and their relations to the excited state dipole moment, Chem. Phys. 67 (1977) 446–457.
[37] L.R. Dalton, A.W. Harper, R. Ghosn, W.H. Steier, M. Ziari, H. Fetterman, R.V. Mustacich, K.-Y. Jen, K.J. Shea, Synthesis and processing of improved organic second-order nonlinear optical materials for applications in photonics, Chem. Mater. 7 (1995) 1060–1081.
[38] M.J. Cho, D.H. Choi, P.A. Sullivan, A.J.P. Akelaitisand, L.R. Dalton, Recent progress in second-order nonlinear optical polymers and dendrimers, Prog. Polym. Sci. 33 (2008) 1013–1058.
[39] D.J. Williams, Organic polymeric and nonpolymeric materials with large optical nonlinearities, Angew. Chem. Int. Ed. Engl. 23 (1984) 690–703.
[40] K. Adjira, M. Sekkal-Rahalb, M. Springborgc, DFT evaluation of structural, electronic and variation properties for complex carbohydrates with biological interest, J. Biomol. Struct. Dyn. 41 (2022) 5981–5989.
[41] Z. Lakbaibi, H. Abou El Makarim, M. Tabyaoui, A. El Hajbi, Study of the solvent effects on the formation of a-bromoglycidic esters in aliphatic series using the quantum DFT method with B3LYP/6–311 G (d, p), J. Mater. Environ. Sci. 8 (1) (2016) 99–115.
[42] M.A. Raza, K. Fatima, Molecular modeling approach for designing of aminoderived anti-Alzheimer agents: a computational study, J. Phys. Org. Chem. e4076 (2020) 1–10.
[43] E. Santamato, Y.R. Shen, Field curvature effect on the diffraction ring pattern of laser beam dressed by spatial self-phase modulation in animatic film, Opt. Lett. 9 (1984) 564–566.
[44] S. Chavez –Cerda, C.M. Nascimento, M.A.R.C. Alencar, M.G.A. da silva, M.R. Mene ghetto, J.M. Hickman, Experimental observation of the Far field diffraction pattern of diveregent and convergent Gaussian beam in a self-defocusing medium, Ann. Opt. XXIX (2006) 1–4.
[45] L. Deng, K. He, T. Zhou, C. Li, Formation and evolution by Far-filed diffraction patterns of divregean and convergant Ganssian beam passing through self-focusing and self-defocusing media, J., Opt. A:Pure Appl. 7 (2005) 409–415.
[46] G.P. Agrawal, Modulation instability induced by cross-phase modulation, Phys. Rev. Lett. 59 (1987) 800–883.
[47] S. Matsuoka, N. Miyanaga, S.A. Mano, M. Naktsuka, Frequency modulation controlled by cross-phase modulation in optical fiber, Opt. Lett. 22 (1997) 25–27.
[48] D.J. Jones, S.A. Diddams, M.S. Taubman, S.T. Cunfiff, L.-S. Ma, J.L. Hall, Frequency comb generation using femtosecond pulses and cross-phase modulation in optical fiber at arbitrary center frequencies, Opt. Lett. 25 (2000) 208–310.
[49] Y. Jia, Y. Shan, L. Wu, X. Dai, D. Fan, Y. Xiang, Broad band nonlinear optical resonance and all-optical switching of liquid phase exfoliated tungsten diselenide, Photo Res. 6 (2018) 1040–1046.
[50] Z. Xue-jun, Y. Zhen-hua, Y. Rui-xin, He Yi-1in, Qin Ying-lin, Xiao Si, He Jun, A review on spatial self- phase modulation of two-dimensiral materials, J. Cent. Soult Univ. 26 (2019) 2295–2306.
[51] Q. Wang, X. Wu, L. Wu, Y. Xiang, Baroadband nonlinear optical respond in Bi_2Se_3-Bi_2-Te_3 deterostructure and it application in all-optical switching, AIP Adv. 9 (2019) 025022 (7PP).
[52] B.L.M. van Baar, J. Rozendal, H. van der Goot, Electron ionization mass spectrometry of curcumin analogues: An olefin metathesis reaction in the fragmentation of radical cations, J. Mass Spectrom. 33 (1998) 319–327.
[53] Y. Cao, R.X. Xu, Z. Liu, A high-throughput quantification method of curcuminoids and curcumin metabolites in human plasma via high-performance liquid chromatography/tandem mass spectrometry, J. Chromatogr. B 949– 950 (2014) 70–78.
[54] S. Gunasekaran, R.A. Balaji, S. Kumeresan, G. Anand, S. Srinivasan, Experimental and theoretical investigations of spectroscopic properties of N-acetyl-5-methoxytryptamine, Can. J. Anal. Sci. Spectrosc. 53 (2008) 149–162.
[55] M.M. Raikwar, L. Rhyman, P. Ramasami, Theoretical Investigation of difluoroboron complex of curcuminoid derivatives with and without phenyl substituent (at meso position): linear and non-linear optical study, ChemistrySelect 3 (2018) 11339–11349.
[56] S. Saravanan, V. Balachandran, Quantum chemical studies, natural bond orbital analysis and thermodynamic function of 2,5-dichlorophenylisocyanate, Spectrochim. Acta Part A: Mol. Biomol. Spectrosc. 120 (2014) 351–364.
[57] Y. Dwivedi, G. Tamashiro, B.L. De, S.C. Zilio, Nonlinear optical characterizations of dibenzoylmethane in solution, Opt. Commun. 293 (2013) 119–124.
[58] S.N. Margar, L. Rhyman, P. Ramasami, N. Sekar, Fluorescent difluoroboron-curcumin analogs: An investigation of the electronic structures and photophysical properties, Spectrochim. Acta, Part A: Mol. Biomol. Spectrosc. 152 (2016) 241–251.
[59] R.R. Mallah, D.R. Mohbiya, M.C. Sreenath, S. Chitrambalam, I.H. Joe, N. Sekar, Fluorescent meso-benzyl curcuminoid boron complex: Synthesis, photophysics, DFT and NLO study, Opt. Mater. 84 (2018) 786–794.
[60] R. Fathima, A. Mujeeb, Plasmon enhanced linear and nonlinear optical properties of natural curcumin dye with silver nanoparticles, Dyes Pigm 189 (2021) 109256.
[61] F.Z. Henaria, S. Cassidy, Nonlinear optical studies of curcumin metal derivatives with cw laser, AIP Conf. Proc. 1653 (2015), 020044 (11 pp).
[62] Sergio E. Torres, Rosario López, Maria D. Sotomayor, Juan C. Tuesta, Gino Picasso, Sabir Khan, Synthesis, characterization, and evaluation of a novel molecularly imprinted polymer (MIP) for selective quantification of curcumin in real food sample by UV-Vis spectrophotometry, Polymers 15 (2023) 2–14.
[63] Z.M. Abou-Gamra, MohamedA. Ahmed, Synthesis of mesoporous TiO_2–curcumin nanoparticles for photocatalytic degradation of methylene blue dye, J. Photochem. Photobio. B: Biol. 160 (2016) 134–141.
[64] Tahseen A. Alsalim, Bahjat A. Saeed, Rita S. Elias, Hanna S. Abbo, Salam J. Titinchi, Synthesis and electronic properties of alkyl- and alkyloxy-curcuminoids, Eur. J. Chem. 4 (2013) 7073.
[65] A.Abu El-Fadl, G.A. Mohamad, A.B.Abd El-Moiz, M. Rashad, Optical constants of Zn1-xLixO films prepared by chemical bath deposition technique, Phys. B 366 (2005) 44–54.
[66] R. Karimzadeh, Spatial self-phase modulation of a laser beam propagation through liquids with self-induced natural convection flow, J. Opt. 14 (2012) 095701 (9 pp).
[67] M.H. Sadr, V.M. Mohammadi, B. Soltani, K. Jamshidi-Ghaleh, S.Z. Mousav, Nonlinear optical responses of $MoS_4Cu_4(PzMe_3)_6C_{l2}$ under low power CW He-Ne laser excitation, Optik 127 (2016) 6050–6055.
[68] M.D. Zidan, M.B. Alsous, A.W. Allaf, A. Allahham, A. AL-Zier, H. Rihawi, Z-scan measurements of the third order optical nonlinearity of C_{60}doped poly (ethylacetylenecarboxylate) under CW regime, Optik 127 (2016) 2566–2569.
[69] K. Kumara, T.C.S. Shetty, S.R. Maidur, P.S. Patil, S.M. Dharmaprakash, Continuous wave laser induced nonlinear optical response of nitrogen doped graphene oxide, Optik 178 (2019) 384–393.
[70] S.R. Maidur, P.S. Patil, Linear optical and third-order nonlinear optical properties of anthracene chalcone derivatives doped PMMA thin films, Optik 190 (2019) 54–67.
[71] M.D. Zidan, A.W. Allaf, A. Allahham, A. Alzier, Investigation of nonlinear optical properties of chromium tetrapyrrole dicarbonyl complex, Optik 200 (2020) 163175 (6 pp).
[72] M. Nadafan, M. Parishani, Z. Dehghania, J.Z. Anvari, R. Malekfar, Third-order nonlinear optical properties of $NiFe_2O_4$ nanoparticles by Z-scan technique, Optik 144 (2017) 672–678.
[73] N. Faraji, W. Mahmood Mat Yunus, A. Kharazmi, Elias Saion, Third-order nonlinear optical properties of silver nanoparticles mediated by chitosan, Optik 125 (2014) 2809–2812.
[74] M. Rashidian, D. Dorranian, S.A. Darani, S. Saghafi, M. Ghoranneviss, Nonlinear responses and optical limiting behavior of Basic Violet 16 dye under CW laser illumination, Optik 120 (2009) 1000–1006.